Journal of Asian Earth Sciences 121 (2016) 72–83

Contents lists available at ScienceDirect

Journal of Asian Earth Sciences

journal homepage: www.elsevier.com/locate/jseaes

Geochemistry of sediments from the Huaibei Plain (east China): Implications for provenance, weathering, and invasion of the Yellow River into the Huaihe River

Lei Zhang [a,b], Xiaoguang Qin [a,*], Jiaqi Liu [a], Chunqing Sun [a,b], Yan Mu [a], Jinliang Gao [a,b], Wenfeng Guo [a,b], Shikai An [c], Chunhui Lu [c]

[a] Key Laboratory of Cenozoic Geology and Environment, Institute of Geology and Geophysics, Chinese Academy of Sciences, Beijing 100029, China
[b] University of Chinese Academy of Sciences, Beijing 100049, China
[c] National Engineering Laboratory for Ecological Environmental Protection in Coal Mines, Huainan, Anhui 232001, China

ARTICLE INFO

Article history:
Received 8 August 2015
Received in revised form 5 February 2016
Accepted 22 February 2016
Available online 26 February 2016

Keywords:
Geochemical
Recycled loess
Provenance
Weathering
Yellow River
Huaibei Plain

ABSTRACT

The sediments of the Huaibei Plain in semi-humid mid-eastern China represent valuable geological records with respect to eolian–fluvial interactions, depositional environments, and climate change in this region. Provenance and weathering conditions are often reconstructed using sedimentary geochemistry methods. In this study, an 8-m core from Huainan and a set of loess samples from northern and southern China were analyzed for major, trace, and rare earth elements (REEs). Results were compared to determine the samples' provenance. The major, trace, rare earth elements contents, and grain size distribution were found to fluctuate widely in the 2–8 m section of the Huainan core and more narrowly closer to the surface (0–2 m). This suggests a provenance shift at a depth of 2 m. The TiO_2/Al_2O_3, SiO_2/Al_2O_3, Th/Nb, La/Nb values and REE patterns in the upper core (0–2 m) are similar to those found in samples from the Chinese Loess Plateau (CLP). These results suggest that the CLP in northern China is likely to be the primary origin of the upper part (0–2 m) of the Huainan core. Compared with CLP samples, the upper part of the Huainan core exhibits lower K_2O/Al_2O_3 values and higher chemical alteration indices. This is indicative of the material's substantial weathering during transportation and re-deposition and implies that these sediments could reasonably be classified as typical recycled loess. The sediments may have been transported from the CLP to Huainan as Yellow River flood events, probably during the last deglaciation (~13.2 ka) as a result of increased precipitation, along with glacier and snow melt in the upper reaches of the Yellow River catchment during this period. This suggests that the Yellow River may have migrated into the Huaihe River catchment much earlier than the earliest historical records (361 BCE) suggest. The implications of this would be profound with respect to Chinese history.

© 2016 Elsevier Ltd. All rights reserved.

1. Introduction

The Huaibei Plain is an extensive alluvial plain formed by the Huaihe and Yellow Rivers, located in the central part of eastern China. Throughout history, the lower course of Yellow River has frequently changed and at times has invaded the Huaibei Plain (Chen et al., 2012), where it discharged abundant silt from the Chinese Loess Plateau (CLP) (Lu et al., 2013; Cui et al., 2014). Therefore, the Yellow River links the CLP to the Huaibei Plain because it acts as a regional eolian–fluvial source-to-sink depositional system.

In China, loess provenance and weathering have been extensively investigated. For example, studies have focused on the loess-soil sequence from the CLP in northern China (e.g., Liu, 1985; Gallet et al., 1996; Ding et al., 2001; Jahn et al., 2001; Sun, 2002, 2005; Yang et al., 2007b; Liang et al., 2009; Nie and Peng, 2014) and the red earth from southern China (e.g., Chen et al., 2008; Hao et al., 2010; Qiao et al., 2011; Hong et al., 2013). However, a limited number of geochemical studies have focused on the relationship between chemical weathering and provenance in loess and recycled loess in China; most previous studies investigated original loess and single eolian depositional systems. To derive provenance and weathering information from recycled loess, more attention must be concentrated on the eolian–fluvial deposit system in the Huaibei Plain. This eolian–fluvial interaction

* Corresponding author.
E-mail address: xiaoguangqin@mail.iggcas.ac.cn (X. Qin).

http://dx.doi.org/10.1016/j.jseaes.2016.02.008
1367-9120/© 2016 Elsevier Ltd. All rights reserved.

deposit system also has a significant role in understanding the source-to-sink transport patterns in the semi-humid area.

Geochemical analyses have been widely employed to distinguish sediment provenance and weathering from various settings, such as marine, lacustrine, fluvial, and eolian (e.g., Sun, 2002; Das et al., 2006; Jin et al., 2006; Yang et al., 2007b; Awasthi et al., 2014; Horbe et al., 2014; Al-Masrahy and Mountney, 2015; Dou et al., 2015). Jin (1990) researched chemical weathering, heavy-mineral composition and clay-mineral composition by using nine late Cenozoic cores sediments from Huaibei Plain. Additionally, the distribution, particle-size composition, physical and mechanical properties of recently deposited silt in Huaibei Plain has been studied (Wu and Wu, 2014). However, the differences in the geochemical characteristic (e.g., weathering degree) between the Yellow River flood sediments in the Huaibei Plain and original loess are not clear. Sediments from the Huaibei Plain form a valuable geological record that contains information about the age of the first Yellow River invasion into the Huaihe River. The Yellow River has flooded and invaded the Huaihe River many times throughout history (Chen et al., 2012). According to *The Chronicle of Bamboo Book*, the first record of a Yellow River invasion of the Huaihe River drainage basin was in 361 BCE (Yellow River Conservancy Commission, 2001). However, the existence of prehistoric incursions of the Yellow River into the Huaihe River drainage basin is still poorly understood. This is a significant scientific question for understanding the evolution of Huaibei Plain and Yellow River.

In this paper, we present analyses of the major, trace, and REEs found in a cored sample from the Huaibei Plain. Results are compared with those derived from similar tests performed on loess samples from northern and southern China with the aim of determining the provenance of the Huaibei sample. Yellow River flood sediments (recycled loess) were found in the Huaibei sample. The degree of weathering of this recycled loess, as well as potential relationships between the original and recycled loess materials are explored and discussed. Finally, the likely timing of the initial incursion of the Yellow River into the Huaihe River catchment is discussed. This study contributes significantly toward an understanding of the relationship between loess and recycled loess, as well as the role of the Yellow River in influencing the development of the Huaibei Plain.

2. Study area

The Huaibei Plain (32°25′–34°35′N, 114°55′–118°10′E) is located between the Yellow and Huaihe Rivers in Anhui Province of eastern China (Fig. 1). It is an extensive alluvial plain (37,400 km^2) related to these two major rivers and ranges in elevation from 20 to 40 m. The topography trends from high to low from the northwest to the southeast with a slope gradient of 1:8000 (Fig. 1) (Jin, 1990; Wu et al., 2009). The mean annual temperature is 14–15 °C with averages in January and July of −2 °C and 37 °C, respectively. The mean annual precipitation is 750–900 mm; approximately 60% falls in summer (June–September). The mean evaporation reaches 1000–1300 mm, which is higher than the annual precipitation (Jin, 1990; Qi, 2009).

The plain is in a semi-humid region that lies within a transition zone in terms of climate, vegetation, and geography (Jin, 1990). To the south of the plain, lies a region with a hot humid subtropical climate and evergreen forests, while to the north lies a cold dry temperate zone with deciduous forests (Wang et al., 2015). Sediments deposited through the Cenozoic Era are generally several hundred meters to >1 km thick (Xie et al., 2013). Most of the Huaibei Plain is covered by Quaternary sediments, except for a small amount of bedrock exposed in the northeast. The Quaternary sediments primarily consist of alternating layers of clay, silt, sand and gravel (Hu et al., 2014). During the Holocene, several to tens of meters of sediment were deposited because of frequent Yellow River flood events. More than 1000 floods have occurred in the past 4000 years, discharging a large amount of silt sediment into the Huaibei Plain. The surface landscape of the Huaibei Plain is primarily formed by the Yellow River floods plain (Wu et al., 2009).

3. Samples and analytical methods

The 8-m-long core was collected in 2012 in Guqiao town (32°50.123′N, 116°30.167′E), Huainan city in the Huaibei Plain, 30 km north of the Huaihe River in Anhui Province, China. The core was collected using mud-flush rotary drilling techniques, and then was split in half longitudinally in the laboratory, where 79 samples were collected from the center of the core at a sampling interval of 0.10 m. Based on lithology, the Huainan (HN) core can be subdivided into two units: (1) sediments above 2 m core depth are loess-like, whereas (2) sediments from 2 to 8 m core depth are yellow–brown silt and mud (Fig. 2).

Twelve bulk sediments samples were radiocarbon dated. All of the samples were washed with acid and distilled water and then dated using the accelerator mass spectrometry (AMS) radiocarbon method. The positions of these radiocarbon samples were at 0.5, 1.0, 1.5, 2.0, 2.5, 3.0, 3.5, 4.0, 4.5, 5.0, 6.0, and 7.0 m from the top of the core. The AMS samples were measured at the Beta Analytic Radiocarbon Laboratory in the USA. The ^{14}C dates were calibrated using CALIB 6.0 and the northern hemisphere atmospheric ^{14}C calibration dataset IntCal09 (Heaton et al., 2009; Reimer et al., 2009). The ^{14}C data are summarized in Table 1.

The particle-size distribution of the 79 samples was determined with a Malvern Mastersizer 2000 laser particle-size analyzer at the Institute of Geology and Geophysics, Chines Academy of Sciences. First, the samples were pretreated with 10–20 mL of 30% peroxide (H_2O_2), heated to 140 °C to remove organic matter and then added to 10 mL of 10% hydrochloric acid (HCl) to dissolve carbonate. Distilled water was then added to the sample and kept for 24 h to rinse acidic ions. Finally, the samples were mixed with 10 mL of 0.05 M sodium hexametaphosphate [$(NaPO_3)_6$] on an ultrasonic vibrator for 10 min before particle-size analysis. The measurement range of the Mastersizer 2000 is 0.02–2000 μm in grain diameter and the relative error is less than 1% (Xiao et al., 2015; Qin et al., 2005).

All samples for major and trace elements analysis were air dried at 40 °C and finely ground in an agate mortar until the material could be sieved through a 200 mesh sieve.

All of the samples were analyzed for major elements oxides (i.e., SiO_2, Al_2O_3, Fe_2O_3, TiO_2, P_2O_5, MgO, CaO, Na_2O, and K_2O). Major element analyses were performed at the Institute of Geology and Geophysics (Chinese Academy of Sciences, Beijing, China). The major elements were determined by X-ray fluorescence spectrometry. The accuracy of the major elements analytical method was established using eight replicate samples. Analytical precision was better than 2%, except for MnO and P_2O_5, which were occasionally 10%. Loss on ignition (LOI) was determined by weighing the samples before and after 1 h of calcination at 950 °C.

Twelve samples were measured for trace (i.e., Li, Be, Sc, V, Cr, Co, Ni, Cu, Zn, Ga, Rb, Sr, Y, Nb, Mo, Cd, In, Sb, Cs, Ba, Ta, W, Re, Tl, Pb, Bi, Th, U, Zr, Hf) and rare earth elements. All elements were analyzed with an inductively coupled plasma-mass spectrometer (Element, FINNIGAN MAT) using solution methods at the Analytical Laboratory (Beijing Research Institute of Uranium Geology, Beijing, China). Details regarding the analytical techniques are discussed in Yang et al. (2007a). The accuracy of the analytical method was established using two internationally recognized standard reference materials: GSR-2 and GSD-12. If the element content is

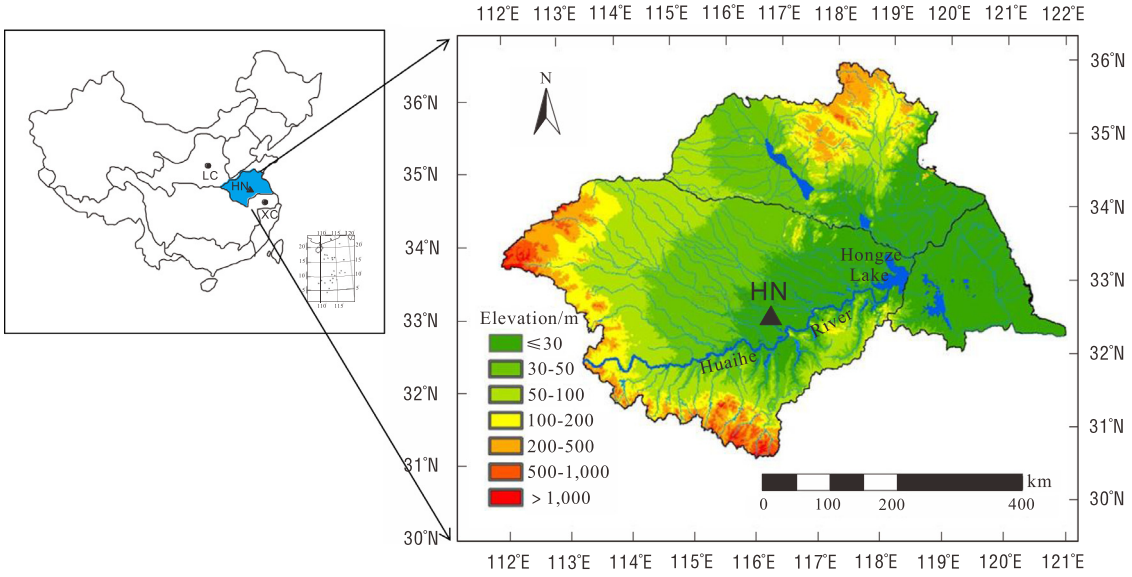

Fig. 1. Digital elevation model of the Huaibei Plain. The solid black triangle indicates the core location.

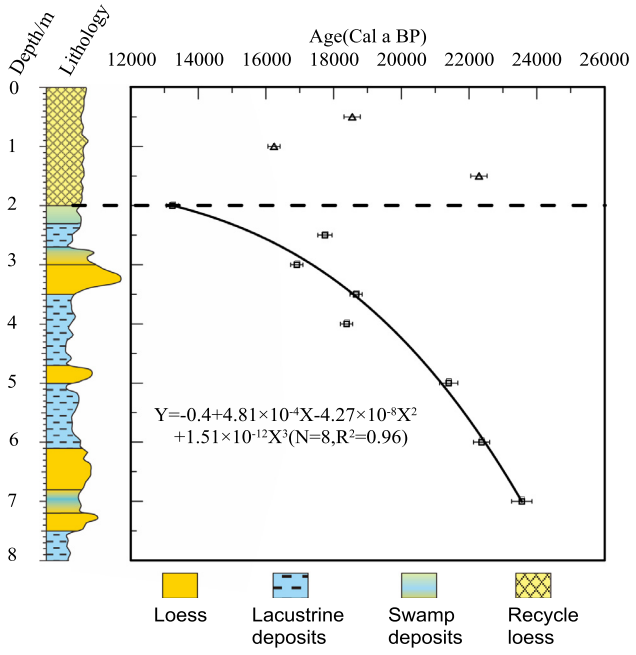

Fig. 2. Lithology and the curve of the calibrated AMS^{14}C ages with sediment core depth.

$>10 \times 10^{-6}$, the accuracy on the measured concentrations is better than 5%; otherwise, if the element content is $<10 \times 10^{-6}$, the accuracy on the measured concentrations is better than 10%.

4. Results

4.1. Dating

Radiocarbon ages from the HN core (Table 1) and the age-depth model (Fig. 2) show that the age from 2 to 8 m is ordered, whereas 0–2 m is disordered. The top three ages will be smaller than the fourth age (13,330–13,130 a BP) in the normal situation; however, all of the top three ages are greater than the fourth and, in fact, none show any sequence. This result might be caused by the Yellow River floods, as they carried old reworded material that covered the surface of the plain. Core chronology was established based on the third polynomial curve using the mean values of the 2σ ranges of the calibrated ages from 2 to 8 m. We use the third polynomial method to establish the age-depth model because the R^2 of the polynomial ($R^2 = 0.96$) is greater than with the linear ($R^2 = 0.89$) method. Polynomial age-depth models are better than linear models at reflecting age trends.

4.2. Sediment grain size and major elements

The median grain size and major elements concentration of the HN core are presented in Fig. 3. The median grain size of the upper 2 m is distributed over a narrow range (12.5–16.9), whereas the 2–8 m exhibits a wide range (4.4–34.6). The major (wt%), trace (ppm), and REE (ppm) concentrations of the HN core sediments are reported in Table 2. Major element oxide changes in the core are shown in Fig. 3. The upper 2 m of the core exhibit a relatively narrow compositional range: SiO_2 (70.37–72.28%, average 71.55%), Al_2O_3 (14.67–15.69%, average 15.02%), TiO_2 (0.79–0.81%, average 0.80%), Fe_2O_3 (5.55–6.44%, average 5.84%), CaO (1.16–1.29%, average 1.25%), K_2O (2.32–2.41%, average 2.37%), MgO (1.43–1.52%, average 1.48%), Na_2O (1.36–1.52%, average 1.46%) (Table 2). In contrast, deeper sediments (2–8 m) show a wider range in SiO_2 (42.29–77.85%, average 66.47%), Al_2O_3 (11.24–19.72%, average 15.86%), TiO_2 (0.62–0.87%, average 0.76%), Fe_2O_3 (3.71–9.81%, average 6.48%), and CaO (1–29.77%, average 4.06%), and a variable compositional range in K_2O (2.24–3.67%, average 2.75%), MgO (1.06–3.15%, average 2.04%), and Na_2O (0.60–2.13%, average 1.33%) (Table 2). Loss on ignition (LOI) varies from 4.81–6.23% (0–2 m) and from 2.4% to 22.92% (2–8 m) (Table 2), reflecting relatively high correlations with carbonate content and hydrous phases, and suggesting that organic matter may also contribute in a minor way. Major element contents of the upper sediments (0–2 m) demonstrate low volatility with little change apparent; however, deeper sediments (2–8 m) show more intense fluctuations (Fig. 2). The uniformity of major element compositions and LOI in the upper 2 m implies the same source area and linked transport processes for this sedimentary package.

In summary, based on lithology, ages, grain size and major element abundances, the HN core can be distinguished into two distinct parts by depth, 0–2 m and 2–8 m.

Table 1
AMS radiocarbon dates of samples from the Huainan (HN) core in the Huaibei Plain (east China).

Laboratory no. Beta-	Sample name	Depth (m)	Dating material	$^{13}C/^{12}C$ ratio (‰)	Conventional radiocarbon age, ^{14}C a BP	Calibrated age ranges, Cal a BP	Sigma (σ)
327085	HN-5	0.5	Organic matter	−20.1	15,180 ± 80	18,600–18,480	2σ
327086	HN-10	1	Organic matter	−20.9	13,230 ± 60	16,560–15,900	2σ
327087	HN-15	1.5	Organic matter	−20.9	18,660 ± 80	22,400–22,170	2σ
327088	HN-20	2	Organic matter	−20.7	11,360 ± 60	13,330–13,130	2σ
327089	HN-25	2.5	Organic matter	−20.2	14,550 ± 70	17,900–17,570	2σ
327090	HN-30	3	Organic matter	−19.1	13,830 ± 60	16,970–16,840	2σ
327091	HN-35	3.5	Organic matter	−20.5	15,440 ± 60	18,720–18,590	2σ
327092	HN-40	4	Organic matter	−21.2	14,920 ± 60	18,490–18,260	2σ
327093	HN-45	4.5	Organic matter	−21.6	20,230 ± 80	24,370–23,930	2σ
327094	HN-50	5	Organic matter	−18.9	17,910 ± 90	21,510–21,270	2σ
327095	HN-60	6	Organic matter	−19.9	18,770 ± 80	22,460–22,260	2σ
327096	HN-70	7	Organic matter	−19.7	19,670 ± 100	23,760–23,340	2σ

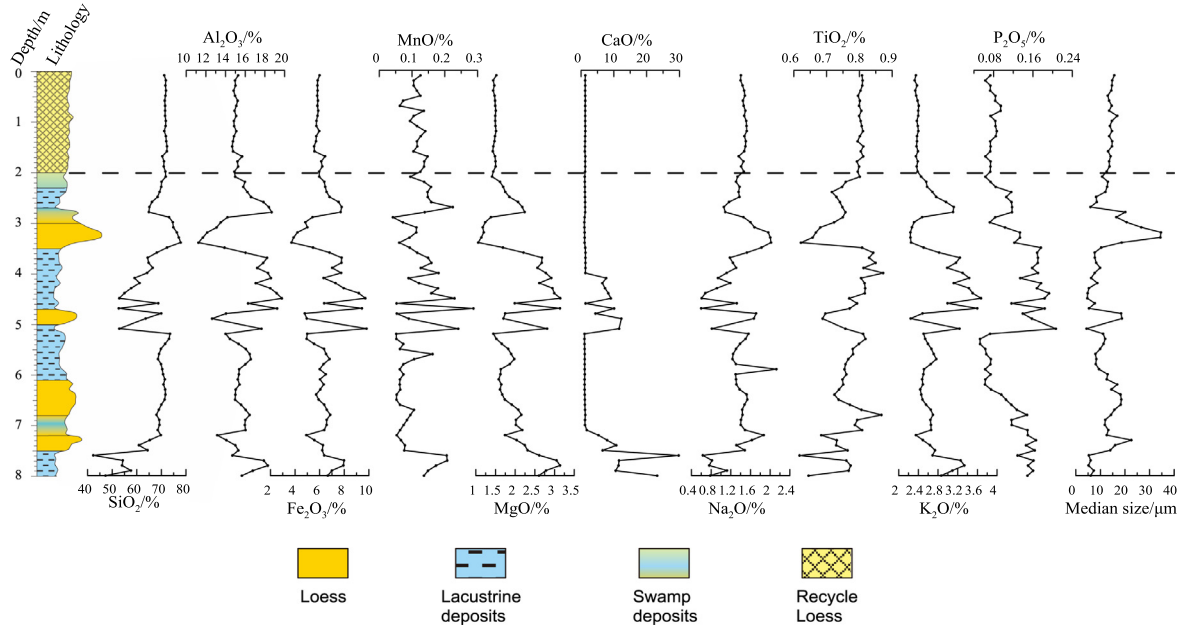

Fig. 3. Changes in major element oxides and median size in the Huainan core from the Huaibei Plain.

4.3. Trace elements

The results of the trace elements analyses are presented in Table 3, and Fig. 4 show the distribution of trace elements in the HN core normalized to the upper continental crust (UCC) (Taylor and McLennan, 1985). In comparison with the UCC (Taylor and McLennan, 1985), the upper 2 m of the HN core is slightly enriched in Zr and Hf, whereas the 2–8 m interval is depleted (with the exception of a few samples). Sr concentrations in upper (0–2 m) and lower (2–8 m) parts range from 118 to 120 ppm (average: 118.8 ppm) and from 118 to 196 ppm (average: 150 ppm), respectively. All Sr values in the lower part are greater than in the upper part with the exception of two samples (Table 3 and Fig. 4). The Rb concentrations are 107–112 ppm for the 0–2 m interval and 79.2–133 ppm for the 2–8 m interval. The Th concentrations in the upper part and lower part range from 13.9 to 14.7 ppm (average: 14.2 ppm) and from 11.2 to 15.8 ppm (average: 13.7 ppm), respectively. The Sc concentration in the upper part and lower part range from 12.5 to 13.3 ppm (average: 12.9 ppm) and from 9.39 to 15.5 ppm (average: 13.2 ppm), respectively. Most of the trace elements, including Zr, Hf, Sr, Rb, Th, Sc and excluding only few (Mo, Cd, W) in the upper part (0–2 m) were concentrated in a narrow range, whereas in the lower part (2–8 m) they were distributed over a wide range (Table 3 and Fig. 4).

4.4. Rare earth elements

The sedimentary REE content is mainly controlled by the lithology of the source area (McLennan, 1989), and therefore is widely

Table 2
Major element concentrations (wt%) of sediments from the Huaibei Plain, recalculated on a volatile-free basis.

	Sample name	Depth (m)	SiO_2	TiO_2	Al_2O_3	Fe_2O_3	MnO	MgO	CaO	Na_2O	K_2O	P_2O_5	Total	CIA	LOI
Upper part 0–2 m	HN-1	0.1	71.15	0.81	15.28	5.99	0.13	1.52	1.29	1.41	2.35	0.07	100	68.06	5.46
	HN-2	0.2	71.82	0.81	14.96	5.84	0.11	1.44	1.24	1.40	2.32	0.06	100	67.89	5.81
	HN-3	0.3	71.63	0.81	15.01	5.82	0.11	1.47	1.27	1.44	2.37	0.07	100	67.44	5.56
	HN-4	0.4	71.87	0.80	14.81	5.83	0.11	1.44	1.24	1.47	2.34	0.07	100	67.27	5.51
	HN-5	0.5	71.64	0.80	14.96	5.80	0.13	1.48	1.27	1.49	2.36	0.08	100	67.21	5.36
	HN-6	0.6	71.36	0.80	15.23	5.86	0.07	1.49	1.28	1.45	2.38	0.08	100	67.63	5.52
	HN-7	0.7	71.51	0.80	15.09	5.81	0.06	1.49	1.26	1.46	2.41	0.09	100	67.38	5.06
	HN-8	0.8	71.51	0.81	14.91	5.88	0.14	1.51	1.27	1.50	2.40	0.09	100	66.94	5.41
	HN-9	0.9	71.49	0.80	15.08	5.83	0.11	1.49	1.26	1.47	2.40	0.07	100	67.35	5.26
	HN-10	1	71.79	0.80	14.84	5.74	0.09	1.49	1.26	1.51	2.37	0.08	100	66.88	5.14
	HN-11	1.1	71.71	0.81	14.87	5.73	0.12	1.50	1.27	1.52	2.39	0.08	100	66.80	5.28
	HN-12	1.2	71.18	0.81	15.09	5.97	0.14	1.51	1.29	1.52	2.40	0.09	100	66.97	6.24
	HN-13	1.3	71.83	0.80	14.86	5.73	0.13	1.49	1.24	1.48	2.37	0.08	100	67.18	5.19
	HN-14	1.4	71.98	0.79	14.75	5.71	0.11	1.47	1.22	1.51	2.37	0.07	100	66.99	4.82
	HN-15	1.5	72.28	0.81	14.67	5.55	0.12	1.44	1.19	1.50	2.36	0.07	100	67.12	4.86
	HN-16	1.6	72.23	0.80	14.76	5.58	0.10	1.43	1.16	1.47	2.39	0.07	100	67.46	5.47
	HN-17	1.7	70.37	0.81	15.69	6.44	0.15	1.49	1.29	1.36	2.35	0.06	100	69.09	5.63
	HN-18	1.8	71.07	0.79	15.20	6.13	0.14	1.50	1.25	1.46	2.39	0.07	100	67.71	5.37
	HN-19	1.9	70.96	0.80	15.28	6.21	0.14	1.50	1.26	1.41	2.37	0.07	100	68.05	5.56
	HN-20	2	71.62	0.79	14.89	5.96	0.13	1.44	1.23	1.46	2.38	0.07	100	67.31	5.38
Lower part 2–8 m	HN-21	2.1	71.77	0.80	14.98	5.97	0.09	1.41	1.12	1.34	2.46	0.06	100	68.49	5.96
	HN-22	2.2	70.07	0.76	15.97	6.37	0.14	1.61	1.14	1.31	2.56	0.07	100	69.56	5.80
	HN-23	2.3	69.95	0.75	15.80	6.45	0.16	1.69	1.16	1.38	2.58	0.08	100	68.80	5.68
	HN-24	2.4	69.27	0.72	16.22	6.56	0.15	1.75	1.18	1.36	2.69	0.12	100	69.00	5.92
	HN-25	2.5	68.44	0.73	16.58	6.80	0.15	1.85	1.20	1.38	2.76	0.11	100	69.07	6.03
	HN-26	2.6	66.16	0.74	17.86	7.54	0.16	2.07	1.23	1.16	2.96	0.12	100	71.74	6.21
	HN-27	2.7	65.13	0.75	18.40	7.79	0.22	2.18	1.23	1.06	3.12	0.12	100	72.85	6.97
	HN-28	2.8	64.92	0.76	18.68	7.70	0.14	2.24	1.25	1.09	3.10	0.12	100	72.91	6.85
	HN-29	2.9	73.11	0.75	14.20	5.42	0.04	1.38	1.08	1.46	2.48	0.08	100	66.83	4.58
	HN-30	3	74.64	0.72	13.51	4.83	0.07	1.24	1.00	1.60	2.31	0.07	100	66.00	4.20
	HN-31	3.1	74.86	0.68	13.09	5.00	0.11	1.18	1.02	1.68	2.27	0.10	100	64.90	3.86
	HN-32	3.2	76.27	0.67	12.14	4.20	0.11	1.20	1.08	1.96	2.24	0.13	100	61.46	3.36
	HN-33	3.3	77.08	0.66	11.69	3.88	0.09	1.14	1.09	2.00	2.24	0.13	100	60.29	2.90
	HN-34	3.4	77.85	0.62	11.24	3.71	0.06	1.06	1.07	2.02	2.25	0.12	100	59.34	2.40
	HN-35	3.5	72.27	0.81	13.89	5.46	0.09	1.69	1.27	1.82	2.51	0.18	100	63.37	4.10
	HN-36	3.6	68.13	0.84	16.03	6.80	0.12	2.21	1.35	1.53	2.82	0.17	100	66.66	5.64
	HN-37	3.7	64.41	0.83	18.22	7.79	0.15	2.68	1.33	1.18	3.24	0.17	100	71.13	6.88
	HN-38	3.8	64.80	0.85	17.83	7.77	0.16	2.68	1.34	1.24	3.16	0.17	100	70.35	6.43
Lower part 2–8 m	HN-39	3.9	66.48	0.81	17.21	7.02	0.13	2.56	1.34	1.31	2.99	0.16	100	69.54	6.28
	HN-40	4	64.21	0.87	18.31	7.75	0.18	2.78	1.32	1.12	3.30	0.17	100	71.65	7.05
	HN-41	4.1	59.11	0.81	18.61	6.32	0.09	2.92	7.65	0.94	3.43	0.13	100	73.22	11.59
	HN-42	4.2	61.12	0.82	17.07	7.29	0.12	2.61	6.49	1.19	3.12	0.18	100	70.06	10.20
	HN-43	4.3	57.73	0.82	18.55	7.95	0.18	2.95	7.31	0.92	3.43	0.17	100	73.37	11.51
	HN-44	4.4	54.96	0.82	19.20	9.18	0.16	2.99	8.31	0.68	3.50	0.19	100	76.09	12.85
	HN-45	4.5	52.89	0.77	19.72	9.71	0.23	3.15	9.07	0.61	3.67	0.18	100	76.74	13.66
	HN-46	4.6	68.73	0.79	16.28	6.37	0.05	1.99	1.35	1.32	2.99	0.12	100	68.21	6.47
	HN-47	4.7	52.67	0.77	19.24	9.44	0.29	3.14	10.08	0.60	3.60	0.18	100	76.65	13.83
	HN-48	4.8	69.96	0.70	14.04	4.79	0.05	1.75	4.38	1.71	2.49	0.14	100	62.77	6.88
	HN-49	4.9	63.59	0.69	12.63	4.95	0.09	1.70	12.28	1.67	2.24	0.16	100	61.46	11.55
	HN-51	5.1	52.89	0.76	17.65	9.81	0.24	2.81	11.59	0.81	3.24	0.21	100	74.05	13.59
	HN-52	5.2	73.51	0.81	14.00	4.99	0.05	1.45	1.05	1.56	2.51	0.07	100	66.07	4.59
	HN-53	5.3	73.11	0.82	14.44	4.94	0.05	1.52	1.03	1.50	2.54	0.05	100	67.08	5.18
	HN-54	5.4	71.51	0.80	15.33	5.55	0.07	1.66	1.05	1.39	2.59	0.05	100	68.65	5.55
	HN-55	5.5	69.81	0.78	16.06	6.35	0.06	1.82	1.09	1.31	2.67	0.06	100	69.62	5.74
	HN-56	5.6	69.05	0.78	16.45	6.52	0.16	1.90	1.12	1.25	2.71	0.07	100	70.10	6.47
	HN-57	5.7	68.60	0.77	16.56	6.81	0.11	1.98	1.11	1.23	2.77	0.07	100	70.19	6.66
	HN-58	5.8	69.85	0.76	16.01	6.31	0.07	1.86	1.09	1.30	2.65	0.07	100	69.57	6.22
	HN-59	5.9	70.36	0.75	15.38	6.00	0.06	1.63	1.10	2.13	2.51	0.06	100	65.17	6.20
	HN-60	6	70.69	0.76	15.35	6.49	0.07	1.63	1.13	1.30	2.50	0.07	100	68.99	5.89
	HN-61	6.1	71.41	0.75	15.24	6.03	0.06	1.58	1.08	1.31	2.48	0.06	100	69.19	5.82
	HN-62	6.2	70.85	0.75	15.42	6.33	0.06	1.65	1.07	1.31	2.49	0.06	100	69.36	6.02
	HN-63	6.3	71.54	0.74	15.02	6.05	0.06	1.61	1.08	1.38	2.44	0.07	100	68.62	5.77
	HN-64	6.4	71.64	0.72	15.00	5.72	0.05	1.67	1.12	1.52	2.46	0.10	100	67.57	5.68
	HN-65	6.5	71.32	0.74	14.97	5.91	0.05	1.74	1.15	1.54	2.48	0.11	100	67.21	5.54
	HN-66	6.6	69.99	0.77	15.58	6.37	0.06	1.91	1.16	1.48	2.56	0.12	100	68.06	6.01
	HN-67	6.7	68.97	0.81	16.04	6.58	0.11	2.08	1.21	1.43	2.65	0.13	100	68.36	5.96
	HN-68	6.8	68.00	0.87	16.45	6.86	0.10	2.16	1.29	1.44	2.70	0.15	100	68.30	6.40
	HN-69	6.9	69.15	0.79	16.01	6.57	0.08	2.02	1.21	1.41	2.64	0.12	100	68.47	6.19
	HN-70	7	69.23	0.79	15.96	6.57	0.07	2.02	1.19	1.40	2.66	0.12	100	68.48	6.33
	HN-71	7.1	68.51	0.81	16.03	6.37	0.06	2.18	1.74	1.49	2.66	0.15	100	67.33	6.37
	HN-72	7.2	69.76	0.68	13.15	4.91	0.05	1.74	5.32	1.87	2.35	0.15	100	60.20	6.92
	HN-73	7.3	65.26	0.73	14.09	5.57	0.07	2.04	7.96	1.63	2.49	0.17	100	63.63	9.37
	HN-74	7.4	60.84	0.73	15.00	6.27	0.08	2.24	10.75	1.31	2.64	0.15	100	67.65	11.83

Table 2 (*continued*)

	Sample name	Depth (m)	SiO_2	TiO_2	Al_2O_3	Fe_2O_3	MnO	MgO	CaO	Na_2O	K_2O	P_2O_5	Total	CIA	LOI
	HN-75	7.5	64.39	0.76	15.30	6.21	0.08	2.31	6.56	1.48	2.74	0.16	100	66.10	9.05
	HN-76	7.6	42.29	0.62	14.69	6.37	0.21	2.61	29.77	0.63	2.69	0.13	100	74.67	22.92
	HN-77	7.7	54.30	0.76	17.89	7.98	0.21	3.05	11.57	0.82	3.26	0.16	100	74.20	14.01
	HN-78	7.8	54.02	0.77	18.29	7.93	0.17	3.14	11.43	0.76	3.34	0.15	100	74.94	14.19
	HN-79	7.9	57.62	0.77	16.77	7.00	0.15	2.78	10.55	1.12	3.09	0.16	100	70.43	12.69
	HN-80	8	47.30	0.65	15.65	6.66	0.14	2.60	23.21	0.78	2.87	0.15	100	73.40	19.91

Table 3
Trace element concentrations (ppm) of Huainan (HN) core sediments from the Huaibei Plain.

Lab. no.	26416	26417	26418	26419	26420	26421	26422	26423	26424	26425	26426	GBW 07104	GBW 07312	UCC
Depth (m)	0.3	0.6	1.2	1.6	2.4	3.2	4.1	4.9	5.7	6.5	7.7			
Sample name	HN-3	HN-6	HN-12	HN-16	HN-24	HN-32	HN-41	HN-49	HN-57	HN-65	HN-77	GSR-2	GSD-12	
Li	36.7	35.3	35.6	38.1	48.1	25.7	46.5	33	46.1	41.2	46.5	18.3	39.0	20
Be	2.08	2.03	2.14	2.11	2.58	1.85	2.3	1.79	2.22	2.05	2.21	1.10	8.20	3
Sc	12.7	13.2	13.3	12.5	15.2	9.39	15.5	11	13.6	12.9	15.1	9.50	5.10	13.6
V	92	91.5	91.4	89.2	103	71.5	103	82.1	105	94	119	94.0	47.0	107
Cr	106	119	111	92	115	137	95.9	89.3	108	120	94.9	32.0	35.0	83
Co	15	12.9	18.3	14	18.8	14.1	14.3	12.8	19.6	12.8	23.3	13.2	8.80	17
Ni	38.8	31.7	38.9	32.4	43.2	37	43	33.4	41.3	40	46	17.0	12.8	44
Cu	21.3	23.3	27.3	22.3	31.7	18	33.6	24.2	30.4	25.3	40.7	55.0	1230	25
Zn	62.8	60.3	67.6	58.5	87.5	51.6	98.6	59	76.5	73.3	97.4	71.0	498	71
Ga	17.1	17.4	18.2	17.1	21.6	13.6	19.7	14.2	18.4	17.5	19.4	18.1	14.1	17
Rb	112	109	107	108	116	79.2	133	82.4	121	104	121	38.0	270	112
Sr	118	120	118	119	118	138	161	196	119	132	186	790	24.0	350
Y	27.6	26	28.5	29.1	28.5	24.6	24.5	29.8	26	26.4	23.5	9.30	29.0	22
Nb	16	15.9	16.6	16.2	16.2	13.8	14.4	16.1	20.9	14.8	45.2	6.80	15.4	12
Mo	0.635	0.774	0.695	0.521	0.936	1.37	0.321	0.762	0.754	0.897	0.756	0.54	8.40	1.5
Cd	0.168	0.053	0.192	0.11	0.319	0.152	0.166	0.276	0.097	0.051	0.28	0.061	4.00	0.098
In	0.065	0.062	0.068	0.059	0.081	0.046	0.076	0.055	0.065	0.065	0.081	0.037	0.96	0.05
Sb	1.26	1.31	1.38	1.33	2.06	1.15	1.18	1.26	1.38	1.43	1.69	0.12	24.0	0.2
Cs	9.98	10.5	10.3	10.1	13	5.77	14	7.92	12.6	10.2	13.6	2.30	7.90	4.6
Ba	548	522	535	541	565	503	532	460	551	495	564	1020	206	550
Ta	1.21	1.1	1.15	1.13	1.01	0.947	1.25	1.53	2.96	1.04	7.46	0.40	3.20	1
W	5.22	4.46	4.12	3.36	4.25	6.21	2.47	3.43	3.71	4.88	2.94	0.45	37.0	2
Re	0.008	0.006	0.007	0.006	0.007	0.006	0.007	0.007	0.007	0.007	0.007		0.008	0.0004
Tl	0.676	0.685	0.731	0.69	0.844	0.571	0.805	0.596	0.764	0.726	0.816	0.16	1.76	0.75
Pb	23.5	23	24.9	23.8	34.1	19.8	25.7	19.7	28	24.2	33.5	11.3	285	17
Bi	0.341	0.352	0.361	0.348	0.502	0.232	0.497	0.294	0.423	0.349	0.537	0.081	10.9	0.127
Th	13.9	14	14.7	14.2	14.7	11.2	15.2	11.3	14.4	13.8	15.5	2.60	21.4	10.7
U	2.36	2.42	2.54	2.48	2.71	3.5	2.03	2.29	2.42	2.32	4.14	0.90	7.80	2.8
Zr	252	232	241	239	204	230	132	173	188	204	113	99.0	234	190
Hf	7.45	6.64	7.09	7.1	5.42	6.81	3.91	5.04	5.77	6.26	3.72	2.90	8.30	5.8

The upper continental crust (UCC) values are from Taylor and McLennan (1985) and McLennan (2001).

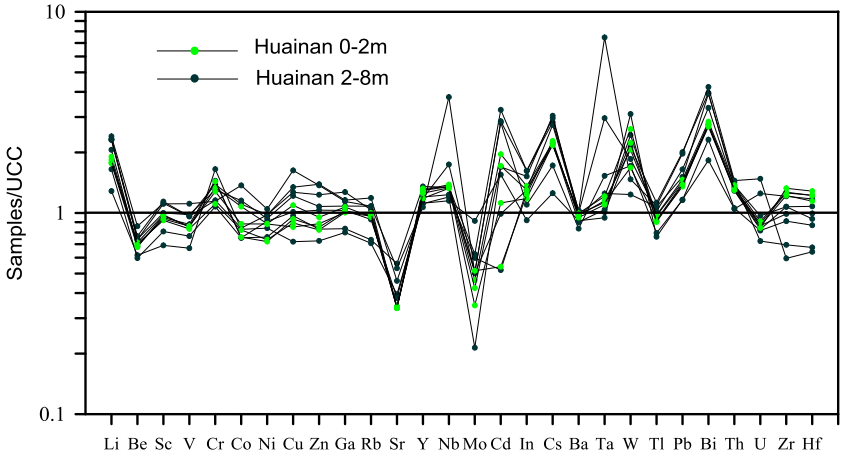

Fig. 4. Upper continental crust (UCC)-normalized spider diagram of trace element composition from the Huainan (HN) core in the Huaibei Plain.

used in sediment provenance studies (e.g., Greaves et al., 1999; Yang et al., 2007a; Újvári et al., 2008; Xie et al., 2014; Asadi et al., 2013; Pan et al., 2014). The REE data of the HN core are presented in Table 4. The Luochuan (LC) (109°25′, 35°45′N) (Gallet et al., 1996) and Xuancheng (XC) (118°51′E, 30°54′N) (Qiao et al., 2011) sections are typical loess sections from the CLP

and lower reaches of the Yangtze River, respectively, and therefore represent typical original loess from northern and southern China. The chondrite-normalized REE patterns (Fig. 5) from the two units in the HN core are similar to those of the LC (Gallet et al., 1996) and XC loess (Qiao et al., 2011), which exhibit enriched light REE (LREE) and relatively flat heavy REE (HREE) profiles, a restricted range of La_N/Yb_N ratios (8–12) and a constant negative Eu anomaly. The average Eu/Eu* values for the 0–2 m and 2–8 m intervals are 0.67 and 0.68, respectively. Both units are similar to LC loess (0.64) (Gallet et al., 1996) and the UCC (0.65) (Taylor and McLennan, 1985; McLennan, 2001) but higher than XC loess (0.58) (Qiao et al., 2011). The average Ce/Ce* values for the 0–2 m and 2–8 m intervals are 0.95 and 0.97, respectively, which is higher than LC loess (0.88) (Gallet et al., 1996), but lower than XC loess (1.10) (Qiao et al., 2011) and the UCC (1.08) (Taylor and McLennan, 1985; McLennan, 2001). The REE patterns for the upper 2 m of the HN core differ from those of the 2 to 8 m section because they exhibit lower $(La/Lu)_N$, $(Ce/Yb)_N$, $(Gd/Yb)_N$, $(La/Yb)_N$, $(La/Sm)_N$, $(Gd/Lu)_N$, and LREE/HREE (Table 4).

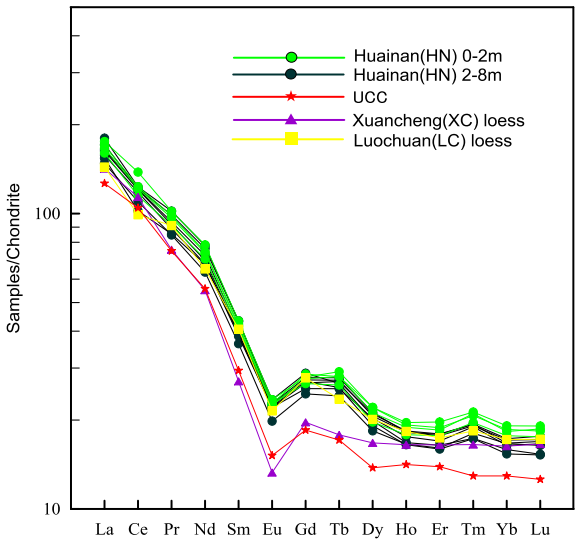

Fig. 5. Chondrite-normalized REE distribution for the Huainan (HN) core, upper continental crust (UCC) values after Taylor and McLennan (1985). The data from the Luochuan loess (LC) are average values from Gallet et al. (1996) and the data from the Xuancheng loess (XC) are average values from Qiao et al. (2011). These three patterns are given as a reference.

5. Discussion

5.1. Sediment provenance and transport processes

The TiO_2/Al_2O_3 ratio is widely used to identify sediment provenance (Sheldon and Tabor, 2009) because Ti is less affected by weathering and usually resides within stable heavy minerals, such as anatase, pyromelane, and rutile (Wen, 1989; Qiao et al., 2011). Al also behaves as a relatively conservative element during weathering (Broecker and Peng, 1982). The TiO_2/Al_2O_3 ratio is not affected by different grain-sizes within silt-sized loess (Gu, 1999; Hao et al., 2010), and therefore it can be used independently to trace the source area of silt-sized loess (Hao et al., 2010). Usually, K_2O/Al_2O_3 is used as a proxy for the chemical maturity of sedimentary units, but can also be used as a sediment provenance index in the early stages of chemical weathering (Cox et al., 1995; Hao et al., 2010). Because quartz tends to be enriched in finer sediment fractions during weathering, Peng and Guo (2001) suggested that SiO_2/Al_2O_3 can be used as a proxy for the provenance of eolian particles; Hao et al. (2010) then used trends in SiO_2/Al_2O_3 vs. TiO_2/Al_2O_3 to trace the source of loess from southern China, because as the transport distance increases, the value of SiO_2/Al_2O_3 will decrease. Figs. 6 and 7 show that the upper part (0–2 m) of the HN core is clearly different from the lower unit (2–8 m) using plots of K_2O/Al_2O_3 vs. TiO_2/Al_2O_3 and SiO_2/Al_2O_3 vs. TiO_2/Al_2O_3. The range of TiO_2/Al_2O_3 (0.065–0.073) is consistent between the loess from the CLP and the upper sediments, implying that its source may from the CLP. The TiO_2/Al_2O_3 (0.05–0.075) from the 2 to 8 m interval shows a wide distribution, suggesting that the provenance of the lower unit may be more complex.

Table 4
Rare earth element concentrations (ppm) from the Huainan (HN) core in the Huaibei Plain.

Element	HN-3	HN-6	HN-12	HN-16	HN-24	HN-32	HN-41	HN-49	HN-57	HN-65	HN-77	GSR-2	GSD-12	UCC
La	40.4	38	41.6	39.5	37.4	35.1	42.7	36.5	39.1	40.6	38.6	22.0	32.7	30
Ce	75.5	70.3	84.6	74.4	72.3	67.2	75.4	62.5	74.1	74.5	73.8	40.0	61.0	64
Pr	9.35	8.66	9.68	9.19	8.44	8.04	9.69	8.11	8.91	9.4	8.73	4.90	6.90	7.1
Nd	34.7	32.8	36.6	34.4	31.6	29.6	36.4	31.5	33.7	35.6	32.4	19.0	26.0	26
Sm	6.46	6.24	6.63	6.36	5.97	5.55	6.59	5.88	6.17	6.64	6.02	3.40	5.00	4.5
Eu	1.32	1.32	1.36	1.3	1.28	1.15	1.36	1.28	1.31	1.32	1.29	1.02	0.61	0.88
Gd	5.88	5.46	5.75	5.67	5.25	5.04	5.92	5.49	5.62	5.72	5.55	2.70	4.40	3.8
Tb	1.05	0.98	1.09	1.05	0.955	0.903	0.996	1.01	1.02	1.04	0.964	0.41	0.82	0.64
Dy	5.38	5	5.6	5.61	5.15	4.67	5.05	5.33	5.24	5.39	4.86	1.85	4.80	3.5
Ho	1.07	1.01	1.09	1.11	0.994	0.938	0.949	1.04	1.03	1.03	0.934	0.34	0.94	0.8
Er	3.06	2.93	3.12	3.26	2.81	2.66	2.72	2.97	2.93	2.96	2.64	0.85	3.10	2.3
Tm	0.54	0.5	0.528	0.543	0.484	0.46	0.442	0.493	0.488	0.494	0.441	0.15	0.53	0.33
Yb	3.11	3.01	3.16	3.25	2.79	2.83	2.7	2.84	2.91	2.94	2.61	0.89	3.70	2.2
Lu	0.47	0.45	0.466	0.485	0.422	0.417	0.389	0.43	0.436	0.448	0.387	0.12	0.58	0.32
$(La/Lu)_N$	9.13	9.13	9.57	8.73	9.50	9.02	11.76	9.10	9.61	9.71	10.69			10.05
$(Ce/Yb)_N$	6.74	6.49	7.44	6.36	7.20	6.60	7.76	6.11	7.07	7.04	7.85			8.08
$(Gd/Yb)_N$	1.56	1.50	1.51	1.44	1.56	1.47	1.81	1.60	1.60	1.61	1.76			1.43
$(La/Yb)_N$	9.32	9.06	9.44	8.72	9.62	8.90	11.34	9.22	9.64	9.91	10.61			9.78
$(La/Sm)_N$	4.04	3.93	4.05	4.01	4.04	4.08	4.18	4.01	4.09	3.95	4.14			4.30
$(Gd/Lu)_N$	1.53	1.51	1.53	1.44	1.54	1.49	1.88	1.58	1.59	1.58	1.77			1.47
ΣLREE	167.73	157.32	180.47	165.15	156.99	146.64	172.14	145.77	163.29	168.06	160.84			132.48
ΣHREE	20.56	19.34	20.80	20.98	18.86	17.92	19.17	19.60	19.67	20.02	18.39			13.89
ΣREE	188.29	176.66	201.27	186.13	175.85	164.56	191.31	165.37	182.96	188.08	179.23			146.37
LREE/HREE	8.16	8.13	8.67	7.87	8.33	8.18	8.98	7.44	8.30	8.39	8.75			9.54
Eu/Eu*	0.65	0.69	0.67	0.66	0.70	0.66	0.67	0.69	0.68	0.65	0.68			0.65
Ce/Ce*	0.95	0.95	1.03	0.96	1.00	0.98	0.91	0.89	0.97	0.94	0.99			1.08

The upper continental crust (UCC) values are from Taylor and McLennan (1985) and McLennan (2001).

Immobile elements, such as REE, Y, Zr, Th, Sc, Nb, trace elements, and their ratios are potential indicators of clastic sediment provenance because their proportions remain unchanged during chemical weathering processes (e.g., Taylor and McLennan, 1985; Bhatia and Crook, 1986; Liu et al., 1993; McLennan et al., 1993; Gallet et al., 1996; Das et al., 2006; Ahmad and Chandra, 2013; Lim et al., 2013; Horbe et al., 2014). The Th/Nb (0.87–0.89) and La/Nb (2.39–2.53) values from 0 to 2 m in the HN core fall within the ranges of northern China loess, which are higher than those of XC loess (Fig. 8). The Th/Nb (0.34–1.06) and La/Nb (0.85–2.97) values of the lower part (2–8 m) are relatively widely distributed with some samples falling within the range of the northern loess field and others seemingly being unrelated to both the northern and southern loess (Fig. 8). This implies that the source conditions of the deeper sediments are more complex.

In addition to the REEs, high field strength elements (Zr and Hf) present in zircons also reflect sediment provenance (Taylor et al., 1983; Taylor and McLennan, 1985). The Zr values for the 0–2 m (4 samples) and the 2–8 m (7 samples) sections of the Huaibei core were 232–252 and 113–230, respectively. The Hf values for the 0–2 m and 2–8 m sections were 6.64–7.45 and 3.72–6.81, respectively (see Table 3). The Zr values with respect to the upper core (0–2 m) were consistently higher than those with respect to the deeper core. Similarly, only one of the Hf values for the upper core was higher than those for the deeper core. The different values for Zr and Hf suggest that zircon concentration differs between the two sedimentary units (Fig. 4). Results thus show that the zircon content of the upper core (0–2 m) is greater than that of the deeper core (2–8 m), which indicates that the upper and deeper core units may have different provenances. Zr is generally abundant in siliceous (quartz rich) rocks. The different range of Zr values between the upper and deeper core sections can be attributed to the fact that the upper core (0–2 m) consists primarily of silty sand (recycled loess) while the deeper core (2–8 m) reflects a varied lithology (Fig. 2). Because Hf exhibits a chemical affinity for Zr, the Hf concentration in a sample depends largely upon the sample's Zr concentration. Thus the variation in both Zr and Hf concentrations between the upper and deeper core sections may be related to the difference in their lithologies, rendering lithology a key component of provenance.

The difference in sediment composition between the two units is also seen in ternary diagrams of Zr/10-Th–Sc (Bhatia and Crook, 1986; Hao et al., 2010; Qiao et al., 2011). Muhs et al. (2008), Hao et al. (2010) and Qiao et al. (2011) have used a similar ternary diagram to determine the provenance of eolian deposits. The upper part (0–2 m) of the HN core falls within the field of northern China loess, and the samples from lower part (2–8 m) also cluster near northern China loess with the exception of two samples (Fig. 9). This result also implies that the provenance of the upper 2 m may be the CLP (north China), whereas the lower unit has two source regions at least. The samples from the lower part (2–8 m) clustering near the northern China loess may originate from the CLP and the two samples from the lower part (2–8 m) that are most different from northern China loess may be representative of another source area.

The TiO_2/Al_2O_3, SiO_2/TiO_2, Th/Nb, La/Nb, and Zr/10-Th–Sc ratios and REE patterns of the upper part (0–2 m) are consistent with loess from the CLP. They indicate that the sediment provenance of the upper part of the HN core is the CLP in northern China. Fig. 10 shows that the HN core was recovered from a paleochannel of the Yellow River, suggesting it may be the mechanism that

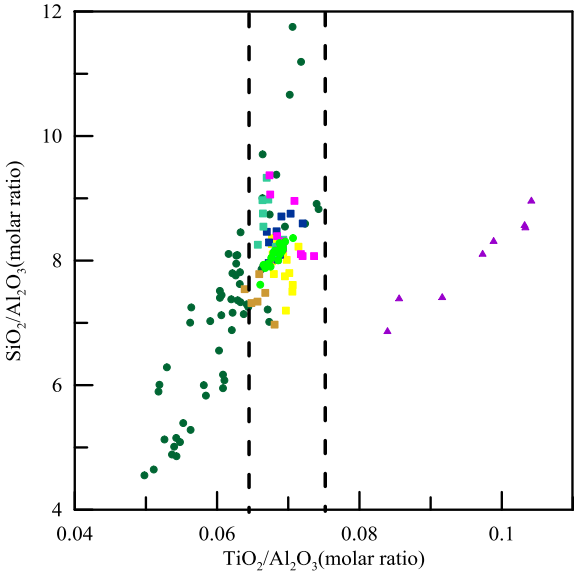

Fig. 7. Cross plot of SiO_2/Al_2O_3 vs. TiO_2/Al_2O_3 of HN core sediments from the Huaibei Plain, and loess from northern and southern China. Data for the Luochuan loess are from Gallet et al. (1996) and Xuancheng and Lingtai loess are from Qiao et al. (2011). Those for the Xining, Xifeng, and Jixian loess are from Jahn et al. (2001). The symbols are the same as in Fig. 6.

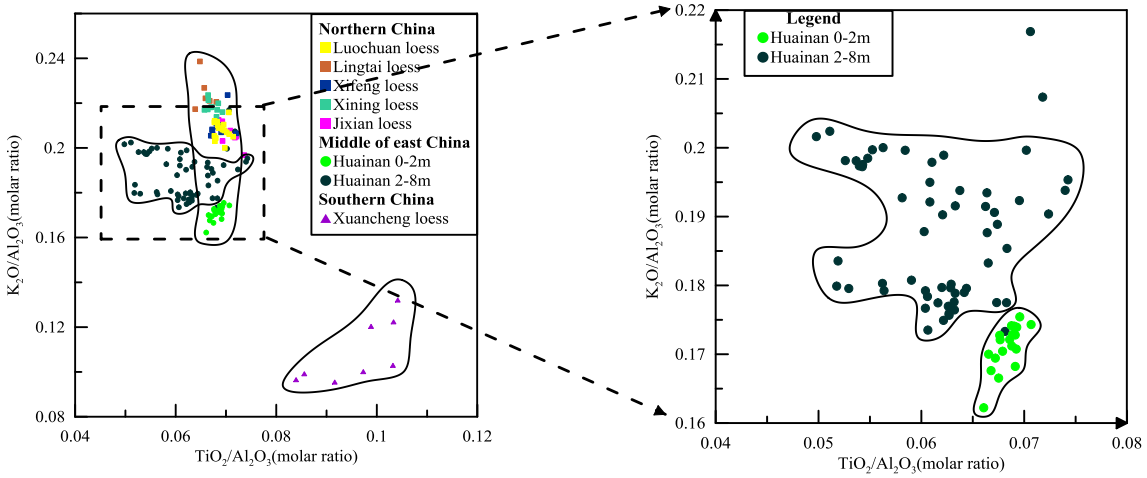

Fig. 6. Cross plots of K_2O/Al_2O_3 vs. TiO_2/Al_2O_3 of Huainan core sediments from the Huaibei Plain, and loess from northern and southern China. Data for the Luochuan loess are from Gallet et al. (1996) and Xuancheng and Lingtai loess are from Qiao et al. (2011). Those for the Xining, Xifeng, and Jixian loess are from Jahn et al. (2001).

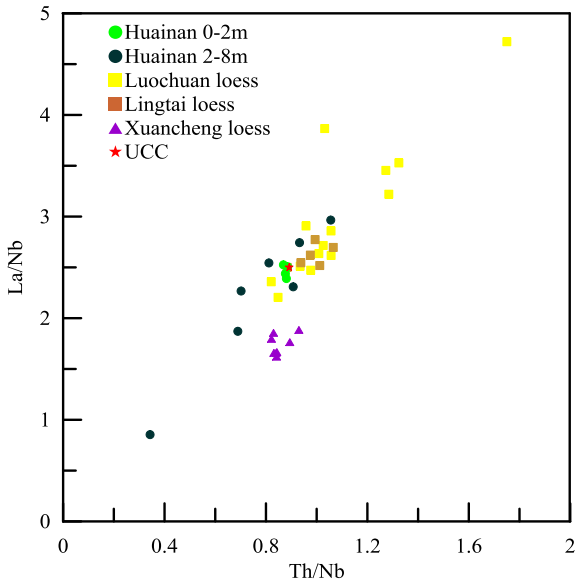

Fig. 8. Plot of immobile trace element ratios for the Huainan core sediments and loess from northern and southern China. Data for the Luochuan loess are from Gallet et al. (1996) and Xuancheng and Lingtai loess are from Qiao et al. (2011).

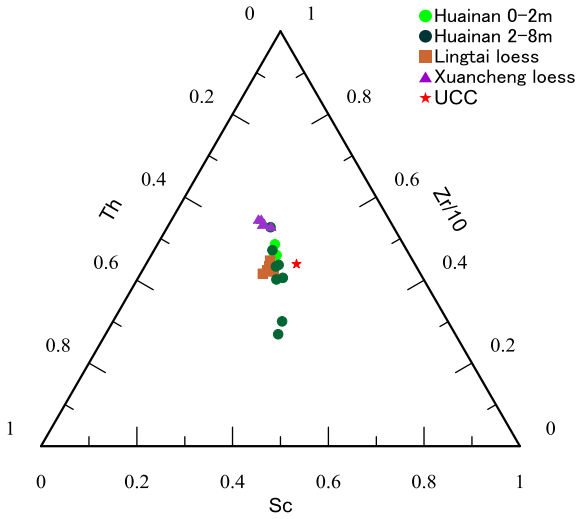

Fig. 9. Ternary plot of Zr/10-Th–Sc for the Huainan core units (0–2, 2–8 m) and loess from northern and southern China. The data for the Xuancheng and Lingtai loess are from Qiao et al. (2011).

delivered loess to this site. Thus, the upper sediments of the HN core might have been transported by the Yellow River from the CLP. According to the provenance and transport process, we suggest that these upper 2 m of sediment are typical recycled loess. Based on lithology and geochemical analyses, the provenance of the lower part (2–8 m) of the core represents mixed loess from northern China and material from the Huaihe River basin.

5.2. Weathering

A Na_2O/Al_2O_3 vs. K_2O/Al_2O_3 diagram (Garrels and Mackenzie, 1971) is used to reflect the removal of Na and K during weathering. Figs. 6 and 11 clearly show K depletion for the upper part of the HN core compared with the lower part. In comparison with the southern and northern loess samples, the K_2O/Al_2O_3 values of the HN core are higher than those of the southern loess but lower than

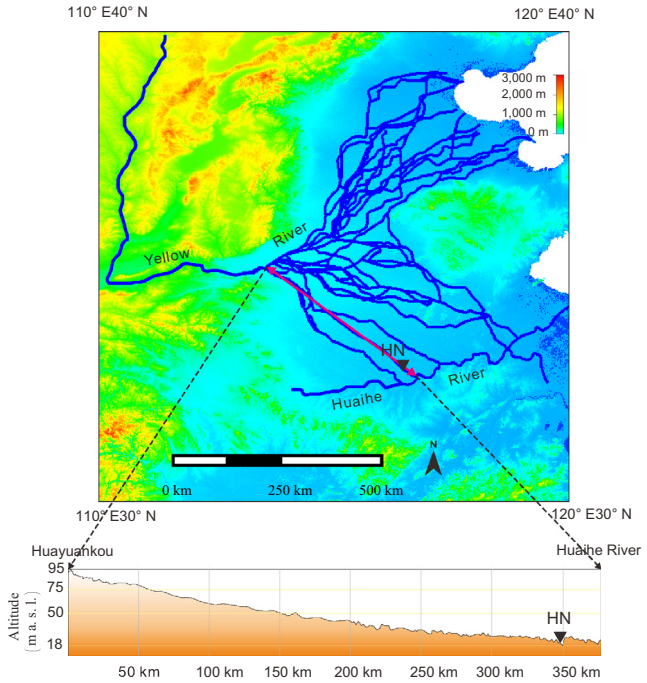

Fig. 10. Changes in the course of the lower Yellow River throughout history and the terrain profile from Huayuankou to the Huaihe River. The channel belts are traced from SRTM data in combination with the Historical Atlas of China (Tan, 1982). Modified from Chen et al. (2012).

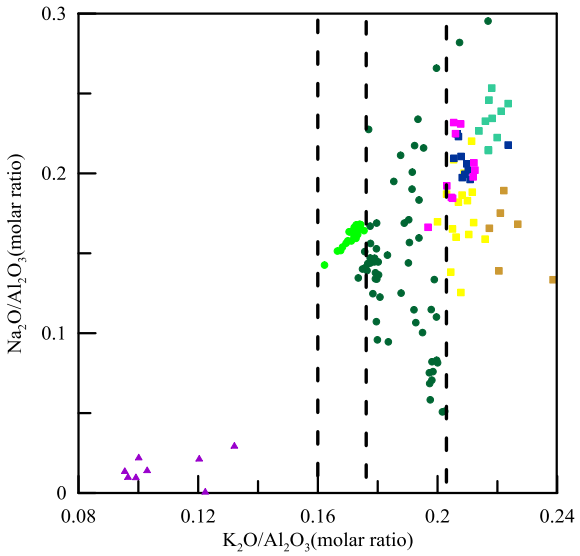

Fig. 11. Cross plot of Na_2O/Al_2O_3 vs. K_2O/Al_2O_3 for the Huainan (HN) core and loess from northern and southern China to illustrate geochemical weathering. Data for the Luochuan loess are from Gallet et al. (1996), Xuancheng and Lingtai loess are from Qiao et al. (2011), and the Xining, Xifeng, and Jixian loess are from Jahn et al. (2001). The symbols are the same as in Fig. 6.

those of the northern loess, with only a few exceptions (Fig. 11). This implies that the weathering overall of the HN core is higher than that of the northern loess but lower than that of the southern loess.

The chemical index of alteration (CIA) is widely used to reflect the degree of weathering (Chen et al., 2008; Nesbitt and Young, 1982) and is expressed as:

$$CIA = (Al_2O_3/(Al_2O_3 + CaO^* + Na_2O + K_2O)) \times 100,$$

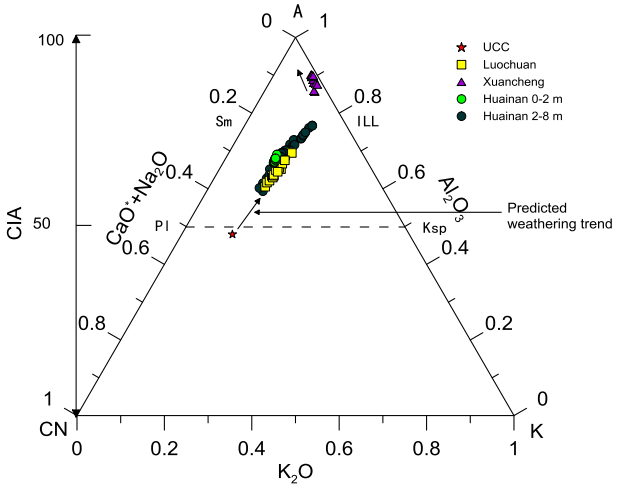

Fig. 12. A–CN–K (Al_2O_3–Na_2O + CaO^*–K_2O) ternary diagram (Nesbitt and Young, 1982, 1989) of the HN core from the Huaibei Plain compared with data for the upper continental crust (UCC) from Taylor and McLennan (1985). Data for the Luochuan (LC) loess from north China are from Gallet et al. (1996) and data for the Xuancheng (XC) loess from south China data are from Qiao et al. (2011).

where CaO^* is the content of CaO incorporated into the silicate fraction and all major oxide units are given in molar proportions. The CaO^* is derived from McLennan (1993).

The CIA values of 20 upper unit (0–2 m) and 59 lower unit (2–8 m) samples of the HN core range from 66.79 to 69.08 (average 67.42) and 59.33–76.73 (average 68.28), respectively. Both ranges and average values are significantly higher than those of the UCC (47.92) and Luochuan (LC) loess (64.66) (Gallet et al., 1996), but significantly lower than those of the Xuancheng (XC) loess (88.78) (Qiao et al., 2011). We can infer that the upper part of the HN core has remained at a constant weathering degree because the CIA range is narrow, but the lower part of the core experienced different weathering processes because the CIA fluctuates with depth. Element mobility during chemical weathering processes and the post-depositional chemical alteration of parent material can also be assessed by plotting the molar proportions of A–CN–K ($A = Al_2O_3$; $CN = Na_2O + CaO^*$; $K = K_2O$) in a ternary diagram (Nesbitt and Young, 1989; Ahmad and Chandra, 2013). This diagram can reflect the chemical weathering trends and variability of both main components and minerals during chemical weathering processes (Chen et al., 2008). The weathering trend line of the HN core nearly parallels that of the A–CN boundary, which is similar to the Luochuan loess (Fig. 12), suggesting that the upper (0–2 m, recycled loess) and lower (2–8 m) parts of the core are in early Na and Ca removal stages. Illite and smectite are the main weathering products, whereas kaolinite was not dominant.

5.3. Dating Yellow River invasions of the Huaihe River

The Yellow River has flooded many times throughout history with documented recordings of more than 1000 floods over the past 4000 years (Shen et al., 1935; Chen et al., 2012). The Yellow River also frequently shifts course in its lower reaches as a result of natural floods and human activity (Milliman and Meade, 1983; Wang et al., 1986; Cui et al., 2014). According to *The Chronicle of Bamboo Book*, the first time the Yellow River made an incursion into the Huaihe River drainage basin as a result of human activity (canal digging) was in 361 BCE, but the first record of a natural invasion was made in 168 BCE (Yellow River Conservancy Commission, 2001). The last time the Yellow River invaded the Huaihe River drainage area was 1938 CE as a result of military sabotage of a dam (Yellow River Conservancy Commission, 2001). However, the timing of the first prehistoric invasion of the Yellow River into the Huaihe River is still unclear. The sediments discharged by the Yellow River floods may thus record information about this incursion. Yang et al. (2000) identified at least six floods over the last 8500 years, with the largest occurring ~7362 a BP. This result indicates that the Yellow River frequently flooded before the instigation of historical records.

Fig. 10 suggests that Yellow River floods may have delivered loess to the HN core site, whereas Fig. 2 shows that the age of the core sediments is both ordered (2–8 m) and disordered (0–2 m). The major and trace elements of the upper unit (0–2 m) sediments are uniform and the degree of weathering is consistent (Figs. 3, 4 and 12), indicating these recycled loess sediments may be paleoflood event deposits. The Yellow River is sourced in the Qinghai–Tibet Plateau, where the temperature and precipitation gradually increased during the last deglaciation (Sowers and Bender, 1995; Thompson et al., 1997; Ji et al., 2005; Peterse et al., 2014; Zhang et al., 2014). Glaciers and snow at the upper reaches of the Yellow River melted and increasing glacially sourced water and rainfall led to a rise in water levels, and floods may have happened in the lower reaches. These floods carried loess from the CLP, invaded the Huaibei Plain and laid the deposits there. Therefore, the age of the first Yellow River invasion into the Huaibei Plain can be inferred from the age of the oldest Yellow River paleoflood, which was determined by ^{14}C as between 13.33 and 13.13 ka (average: 13.23 ka) at 2 m depth (Table 1). We propose that the Yellow River invasion into the Huaihe River drainage basin occurred during the last deglaciation (~13.2 ka), significantly earlier than floods recorded in the earliest historical documents. This result significantly improves our understanding of the evolution of the Huaibei Plain.

6. Conclusions

This geochemical study of the HN core from the Huaibei Plain, and its comparison with the loess from southern and northern China, has led to the following conclusions.

(1) The HN core has uniform compositions of major, trace and rare earth elements in the upper 2 m, but large variability below 2 m.
(2) Major, trace and rare earth element results suggest that the sediment provenance of the HN core shows a suddenly change at 2 m. The primary source of the upper part (0–2 m) of the core was the CLP in northern China. These sediments are typical recycled loess, which were probably transported by a Yellow River flood to the Huaibei Plain. The lower part (2–8 m) shows a mixed loess source from northern China and within the Huaihe River Basin.
(3) The recycled loess sediment is differentiated from the CLP by higher CIA and lower K_2O/Al_2O_3 values. They show similar TiO_2/Al_2O_3, SiO_2/Al_2O_3, Th/Nb, and La/Nb values and REE patterns.
(4) The basal age of the recycled loess indicates that the Yellow River invaded the Huaihe River drainage basin during the last deglaciation (~13.2 ka) at least, which is much earlier than the earliest historic record of 361 BCE. This result demonstrates that the influence of the Yellow River in the formation and shaping of the Huaibei Plain has been underestimated.

Acknowledgements

Financial support for this study was provided by the National Scientific Foundation of China (Grant Nos. 41372187, 41172158,

40472094 and 40024202), the Key Consultation Program of the Chinese Academy of Engineering (Study of Environment and Development of the Huaihe River Watershed), 973 Program (Grant No. 2010CB950200), the Strategic Priority Research Program of the Chinese Academy of Sciences (Grant No. XDA05120502) and the Knowledge Innovation Program of the Chinese Academy of Sciences (Grant No. KZCX2-YW-Q1-03). Special thanks are expressed to anonymous reviewers and the editor for the constructive comments and suggestions that helped improve an early version of the manuscript.

Appendix A. Supplementary material

Supplementary data associated with this article can be found, in the online version, at http://dx.doi.org/10.1016/j.jseaes.2016.02.008. These data include Google maps of the most important areas described in this article.

References

Ahmad, I., Chandra, R., 2013. Geochemistry of loess-paleosol sediments of Kashmir Valley, India: provenance and weathering. J. Asian Earth Sci. 66, 73–89.
Al-Masrahy, M.A., Mountney, N.P., 2015. A classification scheme for fluvial–aeolian system interaction in desert-margin settings. Aeolian Res. 17, 67–88.
Asadi, S., Moore, F., Keshavarzi, B., 2013. The nature and provenance of Golestan loess deposits in northeast Iran. Geol. J. 48, 646–660.
Awasthi, N., Ray, J.S., Singh, A.K., Band, S.T., Rai, V.K., 2014. Provenance of the Late Quaternary sediments in the Andaman Sea: implications for monsoon variability and ocean circulation. Geochem. Geophys. Geosyst. 15, 3890–3906.
Bhatia, M., Crook, K.W., 1986. Trace element characteristics of graywackes and tectonic setting discrimination of sedimentary basins. Contrib. Miner. Petrol. 92, 181–193.
Broecker, W.S., Peng, T.H., 1982. Tracers in the Sea. Eldigio Press, New York, pp. 1–690.
Chen, Y., Li, X., Han, Z., Yang, S., Wang, Y., Yang, D., 2008. Chemical weathering intensity and element migration features of the Xiashu loess profile in Zhenjiang, Jiangsu Province. J. Geog. Sci. 18, 341–352.
Chen, Y., Syvitski, J.P.M., Gao, S., Overeem, I., Kettner, A.J., 2012. Socio-economic impacts on flooding: a 4000-year history of the Yellow River, China. Ambio 41, 682–698.
Commission, Y.R.C., 2001. The chronicle of events of the Yellow River. Yellow River Water Conservancy Publishing House, Zhengzhou, pp. 1–755 (in Chinese).
Cox, R., Lowe, D.R., Cullers, R., 1995. The influence of sediment recycling and basement composition on evolution of mudrock chemistry in the southwestern United States. Geochim. Cosmochim. Acta 59, 2919–2940.
Cui, B.-L., Chang, X.-L., Shi, W.-Y., 2014. Abrupt changes of runoff and sediment load in the lower reaches of the Yellow River, China. Water Resour. 41, 252–260.
Das, B.K., Al-Mikhlafi, A., Kaur, P., 2006. Geochemistry of Mansar Lake sediments, Jammu, India: implication for source-area weathering, provenance, and tectonic setting. J. Asian Earth Sci. 26, 649–668.
Ding, Z., Sun, J., Yang, S., Liu, T., 2001. Geochemistry of the Pliocene red clay formation in the Chinese Loess Plateau and implications for its origin, source provenance and paleoclimate change. Geochim. Cosmochim. Acta 65, 901–913.
Dou, Y., Yang, S., Lim, D.-I., Jung, H.-S., 2015. Provenance discrimination of last deglacial and Holocene sediments in the southwest of Cheju Island, East China Sea. Palaeogeogr. Palaeoclimatol. Palaeoecol. 422, 25–35.
Gallet, S., Jahn, B.-M., Torii, M., 1996. Geochemical characterization of the Luochuan loess-paleosol sequence, China, and paleoclimatic implications. Chem. Geol. 133, 67–88.
Garrels, R.M., Mackenzie, F.T., 1971. Evolution of Sedimentary Rocks. Norton, New York, pp. 1–397.
Greaves, M., Elderfield, H., Sholkovitz, E., 1999. Aeolian sources of rare earth elements to the Western Pacific Ocean. Mar. Chem. 68, 31–38.
Gu, Z., 1999. Weathering Histories of Chinese Dust Deposits Based on Uranium and Thorium Series Nuclides, Cosmogenic ^{10}Be, and Major Elements. Institute of Geology and Geophysics, Chinese Academy of Sciences, Beijing, China, pp. 1–150 (in Chinese with English abstract).
Hao, Q., Guo, Z., Qiao, Y., Xu, B., Oldfield, F., 2010. Geochemical evidence for the provenance of middle Pleistocene loess deposits in southern China. Quatern. Sci. Rev. 29, 3317–3326.
Heaton, T.J., Blackwell, P.G., Buck, C.E., 2009. A Bayesian approach to the estimation of radiocarbon calibration curves: the IntCal09 methodology. Radiocarbon 51, 1151–1164.
Hong, H., Wang, C., Zeng, K., Gu, Y., Wu, Y., Yin, K., Li, Z., 2013. Geochemical constraints on provenance of the mid-Pleistocene red earth sediments in subtropical China. Sed. Geol. 290, 97–108.
Horbe, A.M.C., da Trindade, I.R., Dantas, E.L., Santos, R.V., Roddaz, M., 2014. Provenance of quaternary and modern alluvial deposits of the Amazonian floodplain (Brazil) inferred from major and trace elements and Pb–Nd–Sr isotopes. Palaeogeogr. Palaeoclimatol. Palaeoecol. 411, 144–154.
Hu, Y., Wang, X., Dong, Z., et al., 2014. Determination of heavy metals in the groundwater of the Huaibei Plain, China, to characterize potential effects on human health. Anal. Lett. 48, 349–359.
Jahn, B., Gallet, S., Han, J., 2001. Geochemistry of the Xining, Xifeng and Jixian sections, Loess Plateau of China: eolian dust provenance and paleosol evolution during the last 140 ka. Chem. Geol. 178, 71–94.
Ji, S., Xingqi, L., Sumin, W., Matsumoto, R., 2005. Palaeoclimatic changes in the Qinghai Lake area during the last 18,000 years. Quatern. Int. 136, 131–140.
Jin, Q., 1990. Quaternary of Huaibei Plain in Anhui Province. Geological Publishing House, Beijing, pp. 1–170 (in Chinese).
Jin, Z., Li, F., Cao, J., Wang, S., Yu, J., 2006. Geochemistry of Daihai Lake sediments, Inner Mongolia, north China: implications for provenance, sedimentary sorting, and catchment weathering. Geomorphology 80, 147–163.
Liang, M., Guo, Z., Kahmann, A.J., Oldfield, F., 2009. Geochemical characteristics of the Miocene eolian deposits in China: their provenance and climate implications. Geochem. Geophys. Geosyst. 10, Q04004.
Lim, D., Choi, J.Y., Shin, H.H., Rho, K.C., Jung, H.S., 2013. Multielement geochemistry of offshore sediments in the southeastern Yellow Sea and implications for sediment origin and dispersal. Quatern. Int. 298, 196–206.
Liu, C.-Q., Masuda, A., Okada, A., Yabuki, S., Zhang, J., Fan, Z.-L., 1993. A geochemical study of loess and desert sand in northern China: implications for continental crust weathering and composition. Chem. Geol. 106, 359–374.
Liu, T., 1985. Loess and the Environment. Science Press, Beijing, pp. 1–481 (in Chinese).
Lu, X.X., Ran, L.S., Liu, S., Jiang, T., Zhang, S.R., Wang, J.J., 2013. Sediment loads response to climate change: a preliminary study of eight large Chinese rivers. Int. J. Sedim. Res. 28, 1–14.
McLennan, S., Hemming, S., McDaniel, D., Hanson, G., 1993. Geochemical approaches to sedimentation, provenance, and tectonics. Geol. Soc. Am. Spec. Pap. 284, 21–40.
McLennan, S.M., 1989. Rare earth elements in sedimentary rocks; influence of provenance and sedimentary processes. Rev. Mineral. Geochem. 21, 169–200.
McLennan, S.M., 1993. Weathering and global denudation. J. Geol. 101, 295–303.
McLennan, S.M., 2001. Relationships between the trace element composition of sedimentary rocks and upper continental crust. Geochem. Geophys. Geosyst. 2, 1021.
Milliman, J.D., Meade, R.H., 1983. World-wide delivery of river sediment to the oceans. J. Geol. 91, 1–21.
Muhs, D.R., Budahn, J.R., Johnson, D.L., Reheis, M., Beann, J., Skipp, G., Fisher, E., Jones, J.A., 2008. Geochemical evidence for airborne dust additions to soils in Channel Islands National Park, California. Geol. Soc. Am. Bull. 120, 106–126.
Nesbitt, H., Young, G., 1982. Early Proterozoic climates and plate motions inferred from major element chemistry of lutites. Nature 299, 715–717.
Nesbitt, H., Young, G.M., 1989. Formation and diagenesis of weathering profiles. J. Geol. 97, 129–147.
Nie, J., Peng, W., 2014. Automated SEM–EDS heavy mineral analysis reveals no provenance shift between glacial loess and interglacial paleosol on the Chinese Loess Plateau. Aeolian Res. 13, 71–75.
Pan, B., Guan, Q., Gao, H., Guan, D., Liu, F., Li, Z., Su, H., 2014. The origin and sources of loess-like sediment in the Jinsha River Valley, SW China. Boreas 43, 121–131.
Peng, S., Guo, Z., 2001. Geochemical indicator of original eolian grain size and implications on winter monsoon evolution. Sci. China, Ser. D Earth Sci. 44, 261–266.
Peterse, F., Martínez-García, A., Zhou, B., Beets, C.J., Prins, M.A., Zheng, H., Eglinton, T.I., 2014. Molecular records of continental air temperature and monsoon precipitation variability in East Asia spanning the past 130,000 years. Quatern. Sci. Rev. 83, 76–82.
Qi, H., 2009. Analysis of precipitation changes in Huaibei Plain over last 50 years. Chin. J. Agrometeorol. 30, 138–142 (in Chinese with English abstract).
Qiao, Y., Hao, Q., Peng, S., Wang, Y., Li, J., Liu, Z., 2011. Geochemical characteristics of the eolian deposits in southern China, and their implications for provenance and weathering intensity. Palaeogeogr. Palaeoclimatol. Palaeoecol. 308, 513–523.
Qin, X., Cai, B., Liu, T., 2005. Loess record of the aerodynamic environment in the east Asia monsoon area since 60,000 years before present. J. Geophys. Res. Atmos. 110, 211–226.
Reimer, P.J., Baillie, M.G.L., Bard, E., Bayliss, A., Beck, J.W., Blackwell, P.G., Ramsey, C. B., Buck, C.E., Burr, G.S., Edwards, R.L., Friedrich, M., Grootes, P.M., Guilderson, T. P., Hajdas, I., Heaton, T.J., Hogg, A.G., Hughen, K.A., Kaiser, K.F., Kromer, B., McCormac, F.G., Manning, S.W., Reimer, R.W., Richards, D.A., Southon, J.R., Talamo, S., Turney, C.S.M., van der Plicht, J., Weyhenmeye, C.E., 2009. Intcal09 and marine09 radiocarbon age calibration curves, 0–50,000 years cal BP. Radiocarbon 51, 1111–1150.
Sheldon, N.D., Tabor, N.J., 2009. Quantitative paleoenvironmental and paleoclimatic reconstruction using paleosols. Earth Sci. Rev. 95, 1–52.
Shen, Y., Zhao, S., Daolong, Z., 1935. The Chronicle of the Yellow River. Military Committee and Resources Committee of the Republic, Nanjing, China, pp. 1–262 (in Chinese).
Sowers, T., Bender, M., 1995. Climate records covering the last deglaciation. Science 269, 210–214.
Sun, J.M., 2005. Nd and Sr isotopic variations in Chinese eolian deposits during the past 8 Ma: implications for provenance change. Earth Planet. Sci. Lett. 240, 454–466.
Sun, J.M., 2002. Provenance of loess material and formation of loess deposits on the Chinese Loess Plateau. Earth Planet. Sci. Lett. 203, 845–859.
Tan, Q., 1982. The Historical Atlas of China, vol. 8. China Cartographic Publishing House, Beijing, China, pp. 1–549 (in Chinese).

Taylor, S., McLennan, S., McCulloch, M., 1983. Geochemistry of loess, continental crustal composition and crustal model ages. Geochim. Cosmochim. Acta 47, 1897–1905.
Taylor, S.R., McLennan, S.M., 1985. The Continental Crust: Its Composition and Evolution. Blackwell, Oxford, pp. 1–312.
Thompson, L.o., Yao, T., Davis, M., Henderson, K., Mosley-Thompson, E., Lin, P.-N., Beer, J., Synal, H.-A., Cole-Dai, J., Bolzan, J., 1997. Tropical climate instability: the last glacial cycle from a Qinghai–Tibetan ice core. Science 276, 1821–1825.
Újvári, G., Varga, A., Balogh-Brunstad, Z., 2008. Origin, weathering, and geochemical composition of loess in southwestern Hungary. Quatern. Res. 69, 421–437.
Wang, J., Liu, G., Lu, L., Zhang, J., Liu, H., 2015. Geochemical normalization and assessment of heavy metals (Cu, Pb, Zn, and Ni) in sediments from the Huaihe River, Anhui, China. Catena 129, 30–38.
Wang, Y., Ren, M., Zhu, D., 1986. Sediment supply to the continental shelf by the major rivers of China. J. Geol. Soc. 143, 935–944.
Wen, Q., 1989. Geochemistry of the Chinese Loess. Science Press, Beijing, pp. 1–285 (in Chinese).
Wu, D., Cao, Y., Zhong, X., Shi, G., Xu, D., Qiu, L., Guo, W., 2009. Distribution, age and genesis of cohesive soil containing calcareous nodules in Huaibei Plain of Anhui Province. Rock Soil Mech. 30, 434–439 (in Chinese with English abstract).
Wu, D., Wu, Z., 2014. Genesis, distribution and engineering characteristics of recently deposited silts in Huaibei Plain. Appl. Mech. Mater. 522–524, 223–226.
Xiao, J., Fan, J., Zhai, D., Wen, R., Qin, X., 2015. Testing the model for linking grain-size component to lake level status of modern clastic lakes. Quatern. Int. 355, 34–43.
Xie, K., Zhang, Y., Yi, Q., Yan, J., 2013. Optimal resource utilization and ecological restoration of aquatic zones in the coal mining subsidence areas of the Huaibei Plain in Anhui Province, China. Desalination Water Treat. 51, 4019–4027.
Xie, Y., Meng, J., Guo, L., 2014. REE geochemistry of modern eolian dust deposits in Harbin city, Heilongjiang province, China: implications for provenance. Catena 123, 70–78.
Yang, D., Yu, G., Xie, Y., Zhan, D., Li, Z., 2000. Sedimentary records of large Holocene floods from the middle reaches of the Yellow River, China. Geomorphology 33, 73–88.
Yang, X., Liu, Y., Li, C., Song, Y., Zhu, H., Jin, X., 2007a. Rare earth elements of aeolian deposits in Northern China and their implications for determining the provenance of dust storms in Beijing. Geomorphology 87, 365–377.
Yang, X., Zhu, B., White, P.D., 2007b. Provenance of aeolian sediment in the Taklamakan Desert of western China, inferred from REE and major-elemental data. Quatern. Int. 175, 71–85.
Zhang, W., Wu, J., Wang, Y., Wang, Y., Cheng, H., Kong, X., Duan, F., 2014. A detailed East Asian monsoon history surrounding the 'Mystery Interval' derived from three Chinese speleothem records. Quatern. Res. 82, 154–163.